LINEAR B-SPLINE FINITE ELEMENT METHOD FOR THE IMPROVED BOUSSINESQ EQUATION

Qun Lin[1,*], Yong Hong Wu[1], Ryan Loxton[1] and Shaoyong Lai[2]

1. Department of Mathematics and Statistics,

Curtin University of Technology, Western Australia.

2. Department of Economic Mathematics,

South Western University of Finance and Economics,

610074, Chengdu, China.

Abstract: In this paper, we develop and validate a numerical procedure for solving a class of initial boundary value problems for the improved Boussinesq equation. The finite element method with linear B-spline basis functions is used to discretize the non-linear partial differential equation in space and derive a second order system involving only ordinary derivatives. It is shown that the coefficient matrix for the second order term in this system is invertible. Consequently, for the first time, the initial boundary value problem can be reduced to an explicit initial value problem to which many accurate numerical methods are readily applicable. Various examples are presented to validate this technique and demonstrate its

*Corresponding Author: Q.Lin@curtin.edu.au

capacity to simulate wave splitting, wave interaction and blow-up behavior.

Keywords: Improved Boussinesq equation; Galerkin method; Finite element method; Soliton solution.

1 Introduction

The Boussinesq equation was first introduced in the 1870s by Joseph Boussinesq to model the propagation of shallow water waves in multiple directions. Subsequently, it was applied to many other areas of mathematical physics dealing with wave phenomena [13–16]. Applications to acoustic waves, ion-sound waves, plasma and non-linear lattice waves, are described in references [8, 9, 17, 18].

A general form for the Boussinesq-type equations considered in these references is

$$u_{tt}(x,t) = u_{xx}(x,t) + qu_{xxxx}(x,t) + \left(u^2(x,t)\right)_{xx}, \tag{1.1}$$

where $q = 1$ or -1. The original equation used by Boussinesq in [3] was (1.1) with $q = 1$. In the literature, it is known as the "bad" Boussinesq equation. Equation (1.1) with $q = -1$ is typically called the "good" Boussinesq equation.

Bogolubsky in [1, 2] has shown that the "bad" Boussinesq equation describes non-realistic instability at short wavelengths. Consequently, the following so-called improved Boussinesq equation (IBq) was proposed:

$$u_{tt}(x,t) = u_{xx}(x,t) + u_{xxtt}(x,t) + \left(u^2(x,t)\right)_{xx}. \tag{1.2}$$

Equation (1.2) is more effective for computer simulation than its predecessor. It has been used to model ion-sound wave propagation [18], non-linear wave dynamics in weakly dispersive media [19], and acoustic waves on elastic rods with a circular cross-section [19]. Wazwaz [20] studied variants of the improved Boussinesq equation and

showed that these non-linear variants give rise to compact and non-compact physical structures.

It is shown in [2] that, on an unbounded region with boundary conditions $u(x,t) \to 0$ as $x \to \pm\infty$, the IBq admits analytical solutions of the form

$$u(x,t) = \alpha \mathrm{sech}^2\Big(\frac{1}{\beta}\sqrt{\frac{\alpha}{6}}\,(x - \beta t - x_0)\Big), \tag{1.3}$$

where x_0 is the initial position of the solitary wave, $\alpha > 0$ is the wave amplitude and $\beta = \pm\sqrt{1 + \frac{2}{3}\alpha}$ is the wave speed. The validity of (1.3) is expected to hold for bounded regions which are sufficiently large.

Iskandar and Jain [12] were the first to investigate the IBq numerically. Using a linearization technique and finite difference approximations, a three-level iterative scheme with second order local truncation error was derived. The scheme was used to investigate head-on collisions between solitary waves. Later, Zoheiry [10] developed an improved scheme with a Crank-Nicolson modification. For this scheme, each time step is accompanied by an iterative process that ensures the accuracy requirements are satisfied. Hence, whilst accuracy is maintained, efficiency is compromised.

In [11], Adomian's decomposition was applied to the IBq. Using this method, the solution is expressed as a convergent series; an approximation is obtained by truncating the series after a sufficient number of terms. However, the computation of each term in this series is cumbersome, requiring the integration and differentiation of several complex expressions. The symbolic manipulation package Maple was used and numerical results were calculated and compared with the analytical solution, but only for a very small value of t. It remains to be seen how this method performs for large values of t. In fact, in order to maintain accuracy as t increases, it is expected that a large number of more complicated terms will need to be calculated.

Bratsos [4] considered the IBq with boundary conditions imposed on the first spatial derivative. Finite difference approximations were used to reduce the IBq to a system of ordinary differential equations. Using a Padè approximation, a three level implicit

time-step scheme was developed. Relevant stability bounds were also derived. In addition, Bratsos has employed an implicit finite-difference method to solve the improved Boussinesq equation in [23].

In this paper, we develop a Galerkin-based finite element method for a class of initial boundary value problems governed by the IBq. The spatial axis is partitioned into a set of finite elements and the solution is expressed in terms of linear B-spline basis functions. On this basis, a system involving only ordinary derivatives is obtained. Then, the structure of the system coefficient matrices is exploited to transform the problem into an explicit initial value problem. Accordingly, many standard numerical integration algorithms are applicable. In this manner, an approximate solution to the problem can be generated. In contrast to existing methods, this method is simple to implement and capable of handling the non-linearity in the governing equation. We present the results of four numerical experiments to validate the method and demonstrate its capability in simulating complex wave phenomena.

2 Problem Statement

Consider the initial boundary value problem consisting of the IBq (1.2), the initial conditions

$$u(x,0) = f(x), \quad u_t(x,0) = g(x), \quad \text{for all } x \in (a,b), \tag{2.1}$$

and the boundary conditions

$$u(a,t) = 0, \quad u(b,t) = 0, \quad \text{for all } t \in (0,\infty), \tag{2.2}$$

where $f : (a,b) \to \mathbb{R}$ and $g : (a,b) \to \mathbb{R}$ are given functions.

For fixed t, we multiply (1.2) by a test function $v \in H_0^1(a,b) = \{w \in L^2(a,b) : w_x \in L^2(a,b), w(a) = w(b) = 0\}$, integrate the product over $[a,b]$ using integration by parts,

and then apply the boundary conditions (2.2) to yield

$$\int_a^b \left(u_{tt}v + u_x v_x + u_{xtt}v_x + (u^2)_x v_x\right) dx = 0, \tag{2.3}$$

where the function arguments are suppressed for clarity. Equation (2.3) is required to hold for all admissible test functions. On this basis, we define the following variational problem.

Problem 1. Find a $u \in H_0^1(a,b)$ such that (2.1) is satisfied and, for each $t > 0$,

$$(u_{tt}, v) + (u_x, v_x) + (u_{xtt}, v_x) + \left((u^2)_x, v_x\right) = 0, \quad \text{for all } v \in H_0^1(a,b), \tag{2.4}$$

where

$$(u, v) = \int_a^b u(x)v(x)dx.$$

3 Numerical Method

We partition the x-axis into N finite elements by choosing a set of evenly-spaced knots $\{x_i\}_{i=0}^N$ such that $a = x_0 < x_1 < \cdots < x_{N-1} < x_N = b$ and $x_{i+1} - x_i = h$, $i = 0, \ldots, N-1$. Consider an approximate solution of Problem 1 of the form:

$$U^N(x,t) = \sum_{i=0}^{N} u_i(t)\phi_i(x), \tag{3.1}$$

where

$$\phi_i(x) = \begin{cases} \dfrac{x - x_{i-1}}{x_i - x_{i-1}}, & x \in [x_{i-1}, x_i], \\ \dfrac{x_{i+1} - x}{x_{i+1} - x_i}, & x \in [x_i, x_{i+1}], \\ 0, & \text{elsewhere.} \end{cases}$$

According to (3.1), $u_i(t) = U^N(x_i, t)$, $i = 0, \ldots, N$.

Applying the boundary conditions (2.2) gives $u_0(t) = 0$ and $u_N(t) = 0$ for all $t \in (0, \infty)$. Hence, (3.1) can be simplified to

$$U^N(x,t) = \sum_{i=1}^{N-1} u_i(t)\phi_i(x). \tag{3.2}$$

We follow the standard Galerkin approach and choose test functions $v = \phi_i$, $i = 1, \ldots, N-1$. On this basis, (2.4) must hold with $v = \phi_i$, $i = 1, \ldots, N-1$. Substituting (3.2) into (2.4) gives

$$\sum_{j=1}^{N-1} \left((\phi_i, \phi_j)\, \ddot{u}_j + \left(\phi_i', \phi_j'\right) u_j + \left(\phi_i', \phi_j'\right) \ddot{u}_j + 2 \sum_{k=1}^{N-1} (\phi_i' \phi_k', \phi_j)\, u_k u_j \right) = 0 \tag{3.3}$$

for each $i = 1, \ldots, N-1$, where $'$ and $\dot{}$ denote differentiation with respect to x and t, respectively.

In matrix notation, the system of equations (3.3) can be written as

$$(A + B)\ddot{\mathbf{U}}(t) + B\mathbf{U}(t) + C\big(\mathbf{U}(t)\big)\mathbf{U}(t) = \mathbf{0}, \tag{3.4}$$

where $\mathbf{0} \in \mathbb{R}^{N-1}$ is a zero vector and $\mathbf{U}(t) = \big[u_1(t), u_2(t), \ldots, u_{N-1}(t)\big]^T$. The $(N-1) \times (N-1)$ matrices A, B and $C\big(\mathbf{U}(t)\big)$ are given as follows:

$$A = \big[(\phi_i, \phi_j)\big] = \frac{h}{6} \begin{bmatrix} 4 & 1 & 0 & \cdots & 0 \\ 1 & 4 & 1 & \cdots & 0 \\ 0 & 1 & 4 & \cdots & 0 \\ \vdots & \vdots & \vdots & \ddots & \vdots \\ 0 & 0 & 0 & \cdots & 4 \end{bmatrix},$$

$$B = \big[(\phi_i', \phi_j')\big] = \frac{1}{h} \begin{bmatrix} 2 & -1 & 0 & \cdots & 0 \\ -1 & 2 & -1 & \cdots & 0 \\ 0 & -1 & 2 & \cdots & 0 \\ \vdots & \vdots & \vdots & \ddots & \vdots \\ 0 & 0 & 0 & \cdots & 2 \end{bmatrix},$$

and

$$
\begin{aligned}
C\big(\mathbf{U}(t)\big) &= \left[2\sum_{k=1}^{N-1}(\phi_i'\phi_k', \phi_j)u_k\right] \\
&= \frac{1}{h}\begin{bmatrix}
2u_1 - u_2 & u_1 - u_2 & 0 & \cdots & 0 \\
u_2 - u_1 & -u_1 + 2u_2 - u_3 & u_2 - u_3 & \cdots & 0 \\
0 & u_3 - u_2 & -u_2 + 2u_3 - u_4 & \cdots & 0 \\
\vdots & \vdots & \vdots & \ddots & \vdots \\
0 & 0 & 0 & \cdots & -u_{N-2} + 2u_{N-1}
\end{bmatrix}.
\end{aligned}
$$

Note that C is a time dependent matrix, whilst A and B are constant. By virtue of the structure of A and B, we have the following theorem.

Theorem 1. *The matrix $A + B$ is invertible.*

Proof. Let $\mathbf{y} \in \mathbb{R}^{N-1}$ be a non-zero vector and define $w(x) = \sum_{i=1}^{N-1} y_i\phi_i(x)$. Then we have

$$
\begin{aligned}
\mathbf{y}^T B\mathbf{y} &= \sum_{i=1}^{N-1}\sum_{j=1}^{N-1} y_i b_{ij} y_j \\
&= \sum_{i=1}^{N-1}\sum_{j=1}^{N-1} y_i \left(\int_a^b \phi_i'(x)\phi_j'(x)dx\right) y_j \\
&= \int_a^b \sum_{i=1}^{N-1}\sum_{j=1}^{N-1} y_i\phi_i'(x)\phi_j'(x)y_j dx \\
&= \int_a^b \left(\sum_{i=1}^{N-1} y_i\phi_i'(x)\right)^2 dx \\
&= \int_a^b \left(w'(x)\right)^2 dx \\
&\geqslant 0.
\end{aligned}
$$

Since w' is piecewise continuous, equality holds if, and only if, $w'(x) = 0$ for all $x \in [a, b]$. Now, since $w(a) = 0$, $w'(x) = 0$ for all $x \in [a, b]$ if, and only if, $w \equiv 0$. This, in turn, requires $\mathbf{y} = \mathbf{0}$, which contradicts the assumption that $\mathbf{y}$ is non-zero. Hence, $\mathbf{y}^T B\mathbf{y} > 0$

for all non-zero $\mathbf{y}$ and so B is positive definite. In a similar manner, one can ascertain the positive definiteness of A. Since both A and B are positive definite, it readily follows that $A+B$ is positive definite and therefore invertible. ■

From Theorem 1, it follows that we can invert the matrix $A+B$ in (3.4) to isolate the second derivative term. Since $A+B$ is tridiagonal, this inversion can be performed efficiently using a special algorithm (see Section 6.6 of [5]). Introducing the new variable $\mathbf{V}(t) = \dot{\mathbf{U}}(t)$, it is clear that the system (3.4) is equivalent to the following first order system of ordinary differential equations:

$$\dot{\mathbf{U}}(t) = \mathbf{V}(t), \tag{3.5}$$

$$\dot{\mathbf{V}}(t) = -(A+B)^{-1}\Big[B\mathbf{U}(t) + C\big(\mathbf{U}(t)\big)\mathbf{U}(t)\Big]. \tag{3.6}$$

Initial conditions for (3.5) and (3.6) are obtained by considering (2.1). As such, we have

$$\mathbf{U}(0) = \big[f(x_1), \ldots, f(x_{N-1})\big]^T \tag{3.7}$$

and

$$\mathbf{V}(0) = \big[g(x_1), \ldots, g(x_{N-1})\big]^T. \tag{3.8}$$

The system of ordinary differential equations (3.5) and (3.6) with initial conditions (3.7) and (3.8) defines a standard initial value problem. This problem can be solved using a standard numerical integration algorithm (for example, a Runge-Kutta method).

4 Numerical Examples

In this section, we implement the procedure developed in Section 3 and solve some concrete example problems. Firstly, in Example 1, we validate the procedure by comparing our numerical results with the exact solution. Then, in Examples 2, 3 and 4, we demonstrate the capacity of this technique to simulate wave splitting, wave interaction and blow-up behavior.

The differential equations (3.5) and (3.6) are solved using the Runge-Kutta-Verner variable step-size method (see Section 5.5 of [5]). Thus, the time-step is actually dynamic and is modified within the preset maximum and minimum bounds to ensure that the given error tolerances are satisfied. In Examples 1, 2 and 3, the error tolerance is 1.0×10^{-7}; in Example 4, it is 1.0×10^{-4}. All program codes for the examples below were written in Fortran 95.

Example 1. (Numerical Validation)

We set $\alpha = 0.5$, $x_0 = 0$ and $\beta = \sqrt{1 + \frac{2}{3}\alpha}$ with

$$f(x) = \alpha \text{sech}^2 \left(\frac{1}{\beta} \sqrt{\frac{\alpha}{6}} (x - x_0) \right)$$

and

$$g(x) = 2\alpha \sqrt{\frac{\alpha}{6}} \text{sech}^2 \left(\frac{1}{\beta} \sqrt{\frac{\alpha}{6}} (x - x_0) \right) \tanh \left(\frac{1}{\beta} \sqrt{\frac{\alpha}{6}} (x - x_0) \right).$$

Under these conditions, the exact solution to Problem 1 is given by (1.3). In applying the procedure of Section 3, we discretize the problem on $x \in [-30, 150]$ using evenly-spaced knots with a distance of h between consecutive nodes. In general, the numerical error will depend on h and the time step size Δt. Here, Δt is chosen automatically by the integration routine to satisfy bounds on the local truncation error, while h is determined through a convergence analysis. The numerical solution is compared with the exact solution at $t = 10$ for different values of h in Table 1. To examine the influence of h on the numerical solutions, Figure 1 shows the convergence process. It is clear that convergence is achieved at $h = 0.1$ $(-\ln(h) = 2.3)$ and thus this value for h is used here and in Examples 2 and 3. To investigate the variation of numerical error with time, we plot the error at two points against time in Figure 2. The time-step

determined by the local truncation error is between 0.25 and 0.7.

Table 1. Comparison of the numerical results and exact solution for Example 1.

	Numerical					Exact
x	h=1.000	h=0.500	h=0.250	h=0.100	h=0.05	
5.0	0.073052	0.071010	0.070492	0.070347	0.070327	0.070320
6.0	0.111137	0.110728	0.110658	0.110641	0.110638	0.110637
7.0	0.165915	0.168348	0.169026	0.169220	0.169248	0.169258
8.0	0.240392	0.246098	0.247597	0.248021	0.248082	0.248102
9.0	0.331384	0.339093	0.341042	0.341589	0.341667	0.341694
10.0	0.423374	0.429964	0.431557	0.431999	0.432062	0.432083
11.0	0.487991	0.490172	0.490623	0.490742	0.490759	0.490765
12.0	0.497708	0.494722	0.493915	0.493686	0.493653	0.493642
13.0	0.447066	0.441326	0.439898	0.439499	0.439442	0.439423
14.0	0.357728	0.352426	0.351142	0.350786	0.350735	0.350718
15.0	0.260700	0.257474	0.256703	0.256489	0.256459	0.256448
$\overline{E}$	0.010309	0.002601	0.000651	0.000105	0.000026	

$\overline{E}=\max\limits_{0\leqslant m\leqslant N}\left\{|U^N(x_m,t)-u(x_m,t)|\right\}$, where $u(x,t)$ is the analytical solution to (1.3).

The wave profile of the numerical solution for $t \in [0, 72]$ is shown in Figure 3. The results are in good agreement with those presented in [2, 4, 10, 12]. The average speed of this solitary wave is 1.1542, which is quite close to the theoretical value of $\sqrt{1+\frac{2}{3}\alpha} = 1.154701$. We note that our numerical method is much more efficient than those presented in the references. For example, using our method, an accuracy of $\overline{E} = 3.96 \times 10^{-4}$ at $t = 72$ is achieved with $0.25 \leq \Delta t \leq 0.7$. In [4], Δt needs to be in the order of 0.001 to generate results of comparable accuracy.

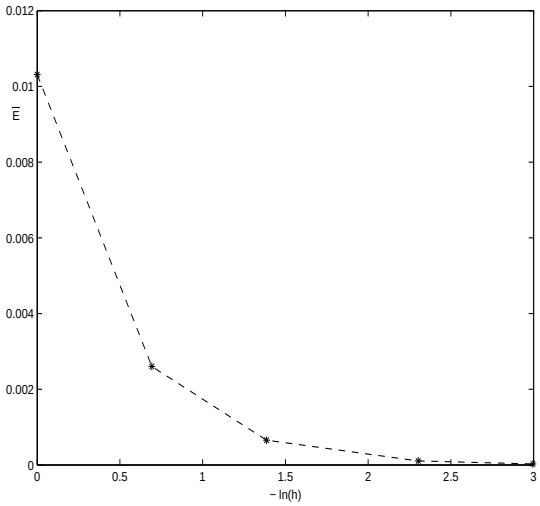

Figure 1: Relationship between h and $\overline{E}$ for Example 1.

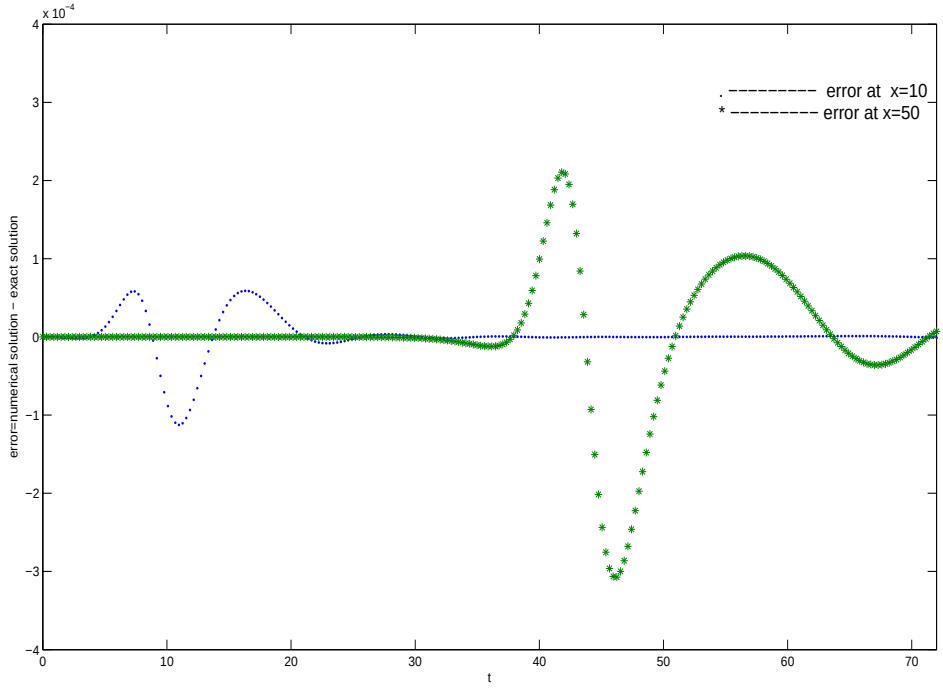

Figure 2: Numerical errors versus time at $x = 10$ and $x = 50$ for Example 1.

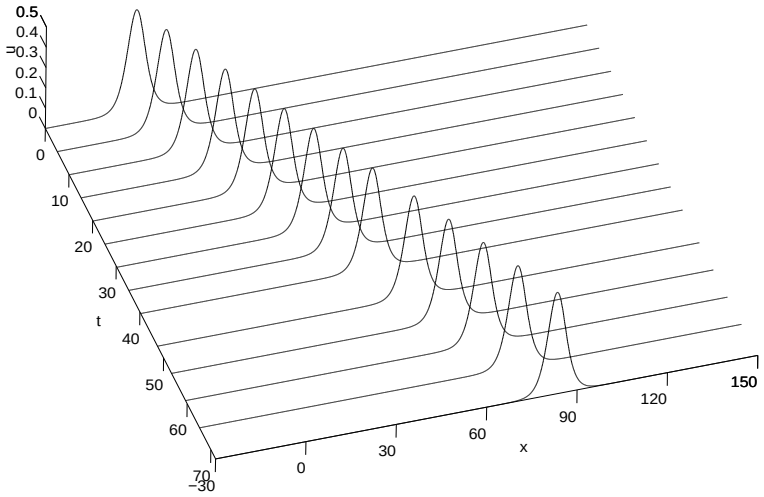

Figure 3: Single soliton solution for Example 1.

The results in Example 1 demonstrate that the method developed in Section 3 is highly accurate for quite moderate time-steps and values of h. Having validated the procedure, we will now present some simulations in the remaining examples.

Example 2. (Wave Break-up)

We consider Problem 1 with $g(x) = 0$ and $f(x)$ defined as in Example 1, where now $x_0 = 30$. This problem is solved on $-30 \leqslant x \leqslant 90$ for $0 \leqslant t \leqslant 40$ using the method of Section 3 with $\Delta t \in [0.25, 0.7]$. The initial stationary wave and the numerical solution are displayed together in Figure 4. The diagram shows the initial stationary wave of amplitude 0.5 breaking into two smaller diverging solitary waves. The break-up is completed at approximately $t = 10$, and the amplitudes of these two solitary waves are approximately equal to 0.26. It is also noted that the solution is symmetric about the plane $x = 30$.

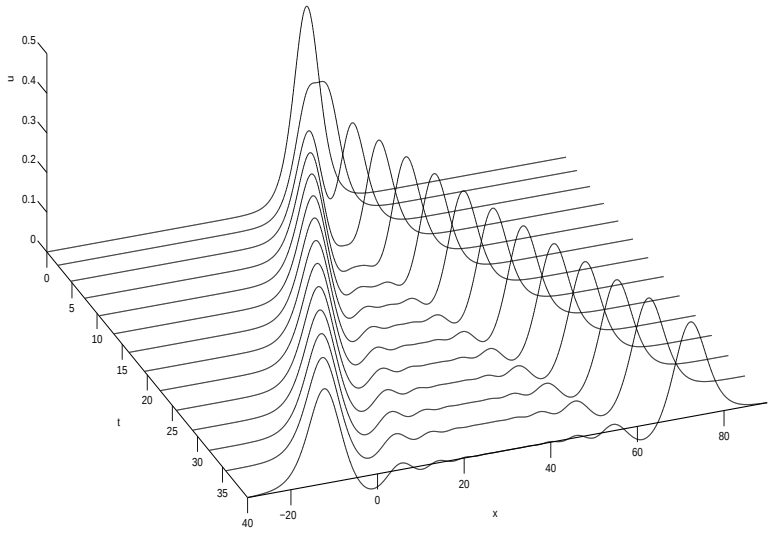

Figure 4: Wave break-up solution for Example 2.

Example 3. (Wave Collision)

As in [12], we investigate the interaction of two IBq soliton waves moving on a collision course. Here, $x \in [-60, 90]$ and $t \in [0, 40]$ with

$$f(x) = \alpha_1 \text{sech}^2\left(\frac{1}{\beta_1}\sqrt{\frac{\alpha_1}{6}}(x + x_0)\right) + \alpha_2 \text{sech}^2\left(\frac{1}{\beta_2}\sqrt{\frac{\alpha_2}{6}}(x - x_0)\right)$$

and

$$\begin{aligned} g(x) = \quad & 2\alpha_1\sqrt{\frac{\alpha_1}{6}}\text{sech}^2\left(\frac{1}{\beta_1}\sqrt{\frac{\alpha_1}{6}}(x + x_0)\right)\tanh\left(\frac{1}{\beta_1}\sqrt{\frac{\alpha_1}{6}}(x + x_0)\right) \\ & -2\alpha_2\sqrt{\frac{\alpha_2}{6}}\text{sech}^2\left(\frac{1}{\beta_2}\sqrt{\frac{\alpha_2}{6}}(x - x_0)\right)\tanh\left(\frac{1}{\beta_2}\sqrt{\frac{\alpha_2}{6}}(x - x_0)\right), \end{aligned}$$

where $\beta_1 = \sqrt{1 + \frac{2}{3}\alpha_1}$, $\beta_2 = \sqrt{1 + \frac{2}{3}\alpha_2}$, $x_0 = 20.0$, $\alpha_1 = 1.0$, $\alpha_2 = 0.5$ and $\Delta t \in [0.15, 0.7]$. Figure 5 displays the head-on collision. The collision starts at approximately $t = 5.29484$. Before the collision of the two waves, the speed and amplitude of one of the waves are 1.28431 and 0.99998, respectively; while the speed and amplitude of the other wave are -1.1521 and 0.49999, respectively. A negative speed indicates that the wave travels in the negative $x-$direction. When the two waves interact, they become a single wave. At approximately $t = 15.95779$, the amplitude of the solitary wave achieves its maximal value of 1.32705. When $t = 22.32919$, the collision is finished, and the amplitude of the larger wave is 0.97714; while the amplitude of the smaller wave becomes 0.49071. According to the contour map in Fig 5, the secondary solitons are visable. Hence, the collision is inelastic. Figure 6 shows another example of inelastic collision in which $x_0 = 20.0$, $\alpha_1 = 0.5$, $\alpha_2 = 2$ and $\Delta t \in [0.09, 0.7]$.

Now, we give some examples of waves of equal magnitude colliding. When $\alpha_1 = \alpha_2 = 0.4$, the collision, shown in Fig 7, is elastic. While $\alpha_1 = \alpha_2 = 1$, the interaction, illustrated in Fig 8, is inelastic. The results are in good agreement with those reported in [23]. However, according to the contour map in Fig 9, the collision with $\alpha_1 = \alpha_2 = 0.5$ is still elastic. Hence, we can conclude that, for the case of equal magnitude

colliding, if the amplitude is less than or equal to 0.5, the collision is elastic.

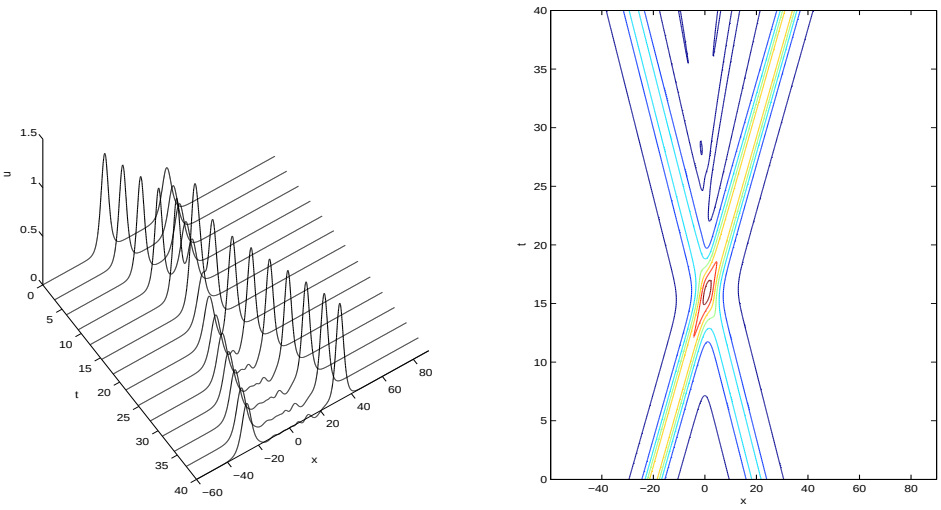

Figure 5: Inelastic collision with $\alpha_1 = 1.0$ and $\alpha_2 = 0.5$ in Example 3. The contour line on the right illustration starts from 0.01 and the level step is 0.2.

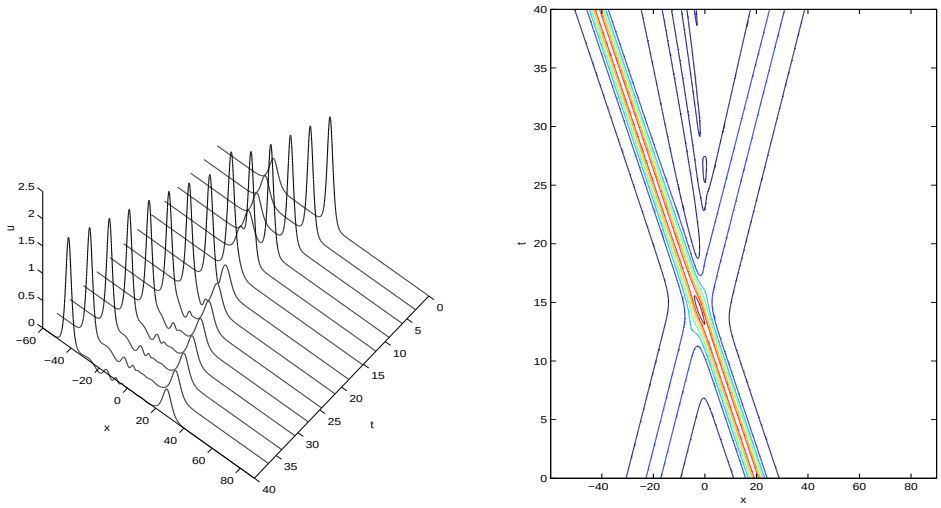

Figure 6: Inelastic collision with $\alpha_1 = 0.5$ and $\alpha_2 = 2.0$ in Example 3. The contour line on the right illustration starts from 0.01 and the level step is 0.3.

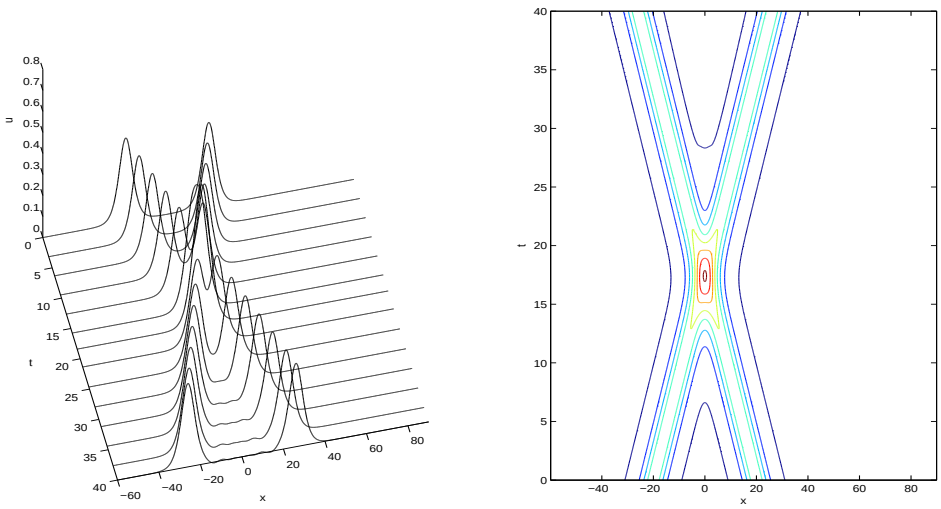

Figure 7: Elastic collision with $\alpha_1 = 0.4$ and $\alpha_2 = 0.4$ in Example 3. The contour line starts from 0.01 and the level step is 0.1.

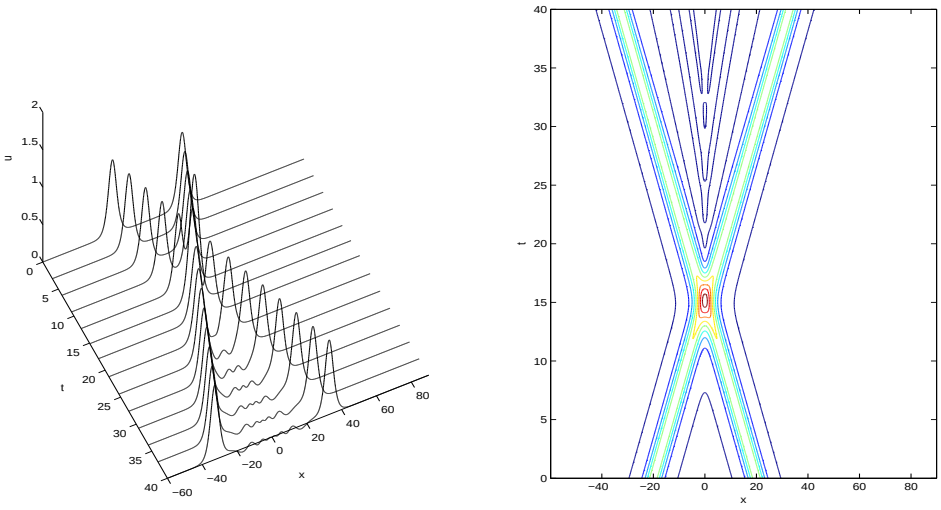

Figure 8: Inelastic collision with $\alpha_1 = 1.0$ and $\alpha_2 = 1.0$ in Example 3. The contour line starts from 0.01 and the level step is 0.2.

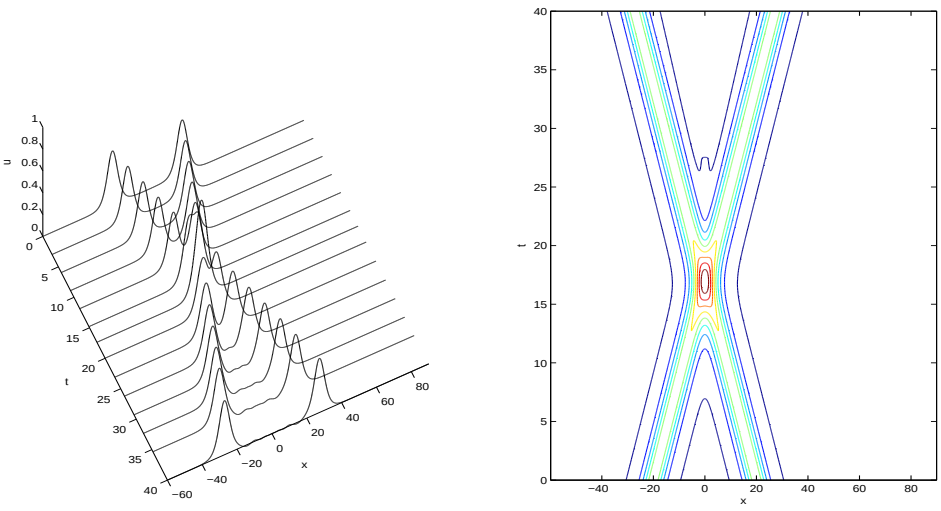

Figure 9: Elastic collision with $\alpha_1 = 0.5$ and $\alpha_2 = 0.5$ in Example 3. The contour line starts from 0.01 and the level step is 0.1.

Example 4. (Solution Blow-up)

In this example, we simulate the solution blow-up discussed in [21, 22]. The IBq (1.2) is considered on $x \in [0, 1]$ with the initial boundary conditions (2.1) and (2.2) defined by $f(x) = -3\sin(\pi x)$ and $g(x) = -\sin(\pi x)$. Under these assumptions, it is known from [21] that there exists a $T^0 > 0$ such that a unique local solution $u \in C^2([0, T^0); H^2(0, 1) \cap H_0^1(0, 1))$ exists, with

$$\|u(\cdot, t)\|_{L^2(0,1)} \to +\infty, \qquad \text{as } t \to T^0,$$

and

$$I(t) = \int_0^1 u(x, t)\sin(\pi x)dx \to -\infty, \qquad \text{as } t \to T^0.$$

To solve this problem numerically using the procedure developed in Section 3, we discretize the space domain into evenly-spaced knots with $h = 0.005$. Note that in this example, we had to set the minimum time-step very small (0.00001) to generate reasonable results until $t = 1.8$. The numerical solution at various values of t is shown in Figure 10. $I(t)$ is tabulated for these values in Table 2.

Table 2. Numerical results for Example 4.

	t=0.0	t=0.58	t=0.99	t=1.50	t=1.60	t=1.70	t=1.80
u(0.5,t)	-3.00	-4.86	-9.97	-65.16	-146.64	-535.13	-131146.69
I(t)	-7.50×10^{-3}	-1.13×10^{-2}	-2.06×10^{-2}	-9.51×10^{-2}	-0.18	-0.49	-30.81

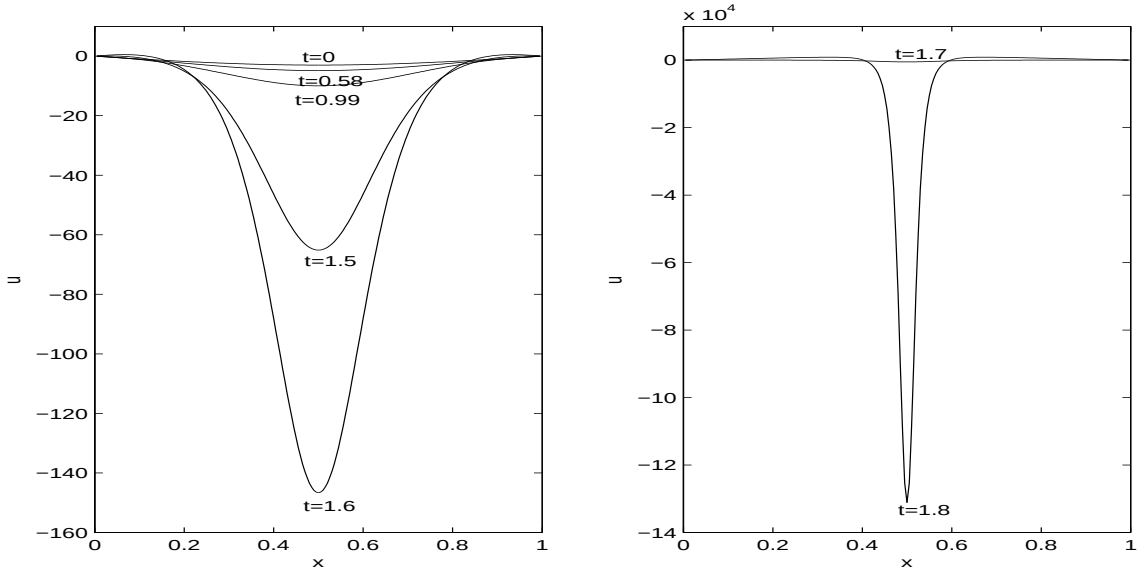

Figure 10: Solution blow-up in Example 4.

5 Conclusion

We have developed an efficient and practical finite element scheme for solving initial boundary value problems for the improved Boussinesq equation. Our numerical results were generated using an adaptive Runge-Kutta-Verner method. This method proved highly accurate. Excellent agreement between the analytical and numerical solutions was obtained in Example 1 for relatively large time-steps, and wave interaction and wave break-up were successfully simulated in Examples 2 and 3. Additionally, we verified numerically a type of solution blow-up that has been shown to exist theoretically. The advantage of our scheme is that it can be implemented easily using existing ordinary differential equation solvers. Many such solvers of excellent quality are available. A special time-stepping scheme does not need to be developed to handle the non-linearity inherent in the Ibq equation.

References

[1] I.L. Bogolubsky, JETP Letters, 24 (1976) 160.

[2] I.L. Bogolubsky, Some examples of inelastic soliton interaction, Computer Physics Communications, 13 (1977) 149-155.

[3] J. Boussinesq, Théorie des ondes et de remous qui se propagent...., Journal de Mathmatiques Pures et Appliques, 17 (1872) 55-108.

[4] A.G. Bratsos, A second order numerical scheme for the improved Boussinesq equation, Physics Letters A, (2007).

[5] R.L. Burden, J.D. Faires, Numerical Analysis, 7^{th} edition, Brooks/cole, (2001).

[6] J.C. Butcher, Numerical Methods for Ordinary Differential Equations, John Wiley & Sons, New York, (2003).

[7] P.L. Christiansen, P.S. Lomdahl, V. Muto, On a toda lattice model with a transversal degree of freedom, Non-linearity, 4 (1990) 477-501.

[8] P.A. Clarkson, M.D. Kruskal, New similarity reductions of the Boussinesq equation, Journal of Mathematical Physics, 30 (1989) 2201-2213.

[9] L. Dehnath, Non-linear PDEs for Scientists and Engineers, Birkhäuser, Boston, (1998).

[10] H. El-Zoheiry, Numerical study of the improved Boussinesq equation, Chaos Solitons and Fractals, 14 (2002) 377-384.

[11] M. Inc, D.J. Evans, A different approach for soliton solutions of the improved Boussinesq equation, International Journal of Computer Mathematics, 81 (3) (2004) 313-323.

[12] L. Iskandar, P.C. Jain, Numerical solutions of the improved Boussinesq equation, Proceedings of the Indian Academy of Sciences (Mathematical Sciences), 89 (1980) 171-181.

[13] S. Lai, Y.H. Wu, The asymptotic solution of the Cauchy problem for a generalized Boussinesq equation, Discrete and Continuous Dynamical Systems - B, 3 (2003) 401-408.

[14] S. Lai, Y.H. Wu, X. Yang, The global solution of an initial boundary value problem for the damped Boussinesq equation, Communications on Pure and Applied Analysis, 3 (2004) 319-328.

[15] S. Lai, Y.H. Wu, B. Wiwatanapataphee, On exact travelling wave solutions for two types of nonlinear $K_{n,n}$ equations and a generalized KP equation, Journal of Computational and Applied Mathematics, 212 (2008) 291-299.

[16] Q. Lin, Y.H. Wu, S. Lai, On global solution of an initial boundary value problem for a class of damped nonlinear equations, Nonlinear Analysis,

[17] F. Lineras, Global existence of small solution for a generalized Boussinesq equation, Journal of Differential Equations, 106 (1993) 257-293.

[18] V.G. Makhankov, Dynamics of classical soliton, Physics Reports (Section C of Physics Letters), 35 (1) (1978) 1-128.

[19] M.P. Soerensen, P.L. Christiansen, P.S. Lomdahl, Solitary waves on non-linear elastic rods. I, Journal of the Acoustical Society of America, 76 (3) (1984) 871-879.

[20] A. -M. Wazwaz, Nonlinear variants of the improved Boussinesq equation with compact and noncompact structures, Computers and Mathematics with Applications, 49 (2005) 565-574.

[21] Z. Yang, Existence and non-existence of global solutions to a generalized modification of improved Boussinesq equation, Mathematical Methods in the Applied Sciences, 21 (1998) 1467-1477.

[22] Z. Yang, X. Wang, Blow up of solutions for improved Boussinesq-type equation, Journal of Mathematical Analysis and Applications, 278 (2003) 335-353.

[23] A.G. Bratsos, A predictor-corrector scheme for the improved , Chaos, Solitons and Fractals (2007), doi:10.1016/j.chaos.2007.09.083.